

RESEARCH ARTICLE

Using transient energy release measurements for the in-line characterization of non-Newtonian fluids and fluid state in pipe flow

 Daniel Ingo Hefft^{1,2}  | Federico Alberini^{1,3}

¹School of Chemical Engineering,
University of Birmingham,
Birmingham, UK

²Product Research, Campden BRI,
Gloucestershire, UK

³Department of Industrial Chemistry
'Toso Montanari', University of Bologna,
Bologna, Italy

Correspondence

Federico Alberini, Department of
Industrial Chemistry 'Toso Montanari',
University of Bologna, Bologna, Viale del
Risorgimento 4, Italy.
Email: federico.alberini@unibo.it

Funding information

Engineering and Physical Sciences
Research Council, Grant/Award Number:
EP/R513167/1

Abstract

Alberini et al. have developed a new technology based on a passive acoustic emission (AE) sensing system that uses only a single sensor, with the goal of providing live and in-situ measurement of rheology. For this study, three different types of fluids were selected to represent common rheological behaviours: Newtonian behaviour, non-Newtonian behaviour with power law, and non-Newtonian behaviour with Herschel–Bulkley relationship. By analyzing the transient energy released during the interaction between the probe and the fluid, distinct acoustic fingerprints were identified in the frequency domain. These acoustic fingerprints were found to be characteristic of the different fluids and their rheology, and were validated in triplicate. Furthermore, the results showed that the intensity of the acoustic emissions increased with higher flow rates (30 to 50 L/min). To test the correlation between flow rate and acoustic response, a neural network regression test was conducted, which demonstrated a direct correlation between AE peaks and flow rate. The neural network used was nonlinear autoregressive network with exogenous inputs (NARX), and the test involved a stepwise regression with 70% training and 30% network validation. The study also introduced the Rheology-AE quotient, which maps fluid constituents against the acoustic signal. Results showed that this was a reliable means of deriving live rheology from a fluid's frequency domain. Finally, the results obtained from this study were validated using an offline rotational rheometer.

KEYWORDS

artificial intelligence, fluid flow, machine learning, passive acoustic sensor technology, rheology, transient energy

Abbreviations: AE, acoustic emission; CFD, computational fluid dynamics; CMC, carboxymethyl cellulose; D, diameter; Exp, experiment; H, height; M, measurement; NARX, nonlinear autoregressive network with exogenous inputs; PIV, particle image velocimetry; SS, stainless steel.

1 | INTRODUCTION

Understanding the rheology of fluids is critical in the manufacturing of various liquid products. This essential quality and product parameter is commonly measured in

This is an open access article under the terms of the [Creative Commons Attribution](https://creativecommons.org/licenses/by/4.0/) License, which permits use, distribution and reproduction in any medium, provided the original work is properly cited.

© 2023 The Authors. The *Canadian Journal of Chemical Engineering* published by Wiley Periodicals LLC on behalf of Canadian Society for Chemical Engineering.

the personal care, petrochemical, pharmaceutical, and food industries.^[1–4] Fluid flow measurements are vital in industrial processes as they enable monitoring of process variation, prediction of production outputs, and accurate metering of fluids during mixing and dosing operations. However, there is often a misconception in the process industry that a fluid passing through a pipe is characterized by a constant viscosity across the pipe's cross-section and length, regardless of whether it is Newtonian or non-Newtonian in rheology. It is well-documented in literature that this is not the case, and that the 3D flow developed in a pipe is highly influenced by the rheology of the fluid.^[5–7]

Rheology can be measured at various stages of production, including assessing raw materials before production, during production, and at the endpoint before packaging/filling. Endpoint rheological measurements are particularly important to ensure that the product meets the target specification and that the consumer receives a product with the desired flow properties. Products with unexpected or undesired rheology, such as those that impair swallowability, are often rejected by consumers, resulting in consumer dissatisfaction, damage to brand reputation, and additional costs for companies in complaint management handling.^[8]

Usually, a distinction is made based on the type of rheometer, and they are classified as off-line (e.g., rotational rheometer), on-line (e.g., melt index determination in polymer industries^[9]), and in-line (e.g., PIV systems^[10]). The most desired type of rheometer would be an in-line rheometer as the results from such a device are the closest possible measurement mode to obtain real-state fluid information. Furthermore, off-line rheometers are very time-consuming and require a high level of skill during setup and operation, while in-line and on-line devices follow a metrological approach. However, off-line rotational rheometers are the most commonly employed type of rheometer in the industry.

Due to a lack of readily available technologies for in-line application on a broad range of fluids and across a broad range of flow rates, the wastage due to faulty rheology is assumed to be in the region of 5%.^[10] To put this into context, let us take a mundane product such as shampoo. The global shampoo market was valued at USD 30.09 billion in 2020, and 55.22% of the shampoos produced globally are liquid (by market share).^[11] The proportion of the market value belonging to liquid shampoo products would be USD 16.62 billion. Assuming the referenced 5% wastage figure, the market potentially lost out on a value of USD 0.83 billion in 2020.

Besides the lost economic benefit, waste has a negative impact on the environment and is costly to dispose of for many chemical substances-based products (such as shampoo).

An ideal in-line rheometry device should meet the following conditions:

- Affordability;
- Capability to work in laminar and turbulent regimen;
- Capability to handle any type of fluid;
- Being accurate and measurements being repeatable;
- High resolution/sensitivity to detect rheological changes;
- Capability to work under harsh conditions (i.e., pH, temperature, pressure);
- Easy to operate;
- Being scalable;
- Easy and flexible in deployment; and
- Meeting hygienic design requirements.

The present study uses a passive acoustic emission (AE) sensing system flanged onto the outer pipe wall of a pipe segment. This pipe segment has a probe inserted into it that serves as a surface on which acoustic emissions can be detected and conveyed to the surface of the sensor (which sits perpendicular to the probe). A detailed description and drawings of the device are given in the IPO filing record WO2020260889A1.^[12] Three Newtonian and seven non-Newtonian fluids (including power law (4) and Herschel–Bulkley (3) models) were tested, each across three flow rates.

The present study investigates the system's capability to detect fluids with different rheological behaviours across different flow rates. The novelty of the approach lies in using a single passive AE sensor that is typically used exclusively for the assessment of solid structures to monitor their integrity and detect brittle material failure.^[13] Compared to the aforementioned technologies, the presented one is capable of distinguishing the type of rheological flow behaviour not only in laminar but also in turbulent regimes. The fundamental principle on which this technology is based is that the flow field influenced by the rheological behaviour of the fluid generates a specific pressure field, which produces the corresponding passive acoustic signal that is unique to the type of rheology and flowing conditions.

(Passive) AEs are sounds generated by various physical and mechanical processes, including the movement of fluids. The relationship between AEs and fluid rheology is a topic of ongoing research.^[5] Despite progress in understanding the relationship between AEs and fluid rheology, there are still significant knowledge gaps that need to be addressed.

One of the main challenges in understanding the relationship between AEs and fluid rheology is the complex nature of fluid flow and the many factors that can influence the generation of AEs. Factors such as the fluid's viscosity, temperature, pressure, and the

presence of solid particles can all play a role in the generation of AEs and their relationship with fluid rheology.^[14]

Another challenge is the difficulty in accurately measuring and characterizing AEs in complex fluid systems. Traditional AE measurement techniques, such as piezoelectric sensors, can be influenced by various factors such as the type of fluid,^[15] the presence of solid particles, and the location of the sensors. Newer, more advanced measurement techniques, such as laser-based sensors for foam rheology,^[16,17] are being developed to address these challenges, but they are still in the early stages of development and have not yet been widely adopted.

There is also a lack of understanding of the fundamental mechanisms by which AEs are generated in fluid systems and how they relate to fluid rheology. Therefore, more research is needed to understand the relationship between AEs and fluid rheology.

Despite significant progress in understanding the relationship between AEs and fluid rheology for multiphase systems (most prominently in the context of bubble assessment), there are still significant knowledge gaps that need to be addressed. Further research is needed to fully understand the complex relationships between AEs and fluid rheology, including the factors that influence the generation of AEs, the development of more accurate measurement techniques, and a deeper understanding of the underlying mechanisms by which AEs are generated in fluid systems.

The results of this study indicate that the system is capable of capturing AEs released by both Newtonian and non-Newtonian rheology fluids. Additionally, the system demonstrates that increases in flow rate are reflected in intensity increases when analyzing the frequency domain. Unlike in the study presented by Hefft and Alberini,^[5] this was accomplished using an obstruction-free fluid system.

2 | INDUSTRIAL IN-LINE RHEOMETRY TECHNIQUES

In-line rheometry has always been a challenge, and there are only limited technologies available to assess fluid rheology live and in-situ. However, there is a desire to have such a live and in-situ fluid rheology metrology device, especially in the formulated liquid product manufacturing sector. These devices are aligned with current industry trends in the personal care sector to make use of Industry 4.0 solutions and have led to major investments in these technologies, respectively.^[18,19]

The following presents two in-line rheology technologies that can be used for the characterization of rheology (no specific order applies).

2.1 | Electrical resistivity tomography (ERT)

Electrical resistivity tomography (ERT) is not a novel technology and was originally designed for geophysics and hydrology, also known as geohydrology.^[20–22] ERT technology typically involves methods for exploring the Earth's crust by measuring electrical voltage and current strength at the Earth's surface. This includes the common setups below:

1. Self-potentials (natural, galvanic elements in ore deposits)^[23];
2. Direct current method^[21]; and
3. Alternating current methods in which electrodes supply artificial currents to the ground.^[23]

The methods that use artificial current supply often use four-point arrangements (two electrodes for supplying the current, two probes for measuring the potential) because this is the only way to eliminate the contact resistance that occurs at the electrodes. When arranging the electrodes in a line (e.g., power supply through the outer electrodes, measurement on the inner electrodes or probes), there are various options, including: Schlumberger method, Wenner method, dipole–dipole array method, and pole–dipole forward and reverse array method.

2.1.1 | The Schlumberger method

Four auxiliary earth electrodes or probes are inserted into the earth in a straight line at a set distance a . An electric current is fed into two electrodes supplied by a single current source. Then, the potential difference (ΔV) between the two inner auxiliary earths is measured with a voltmeter. The value of the resistance R read on the measuring device enables the calculation of the special Earth's resistance ρ_r . This can be expressed by the formula presented by Wenner^[24]:

This is an equation, numbered:

$$\rho_r = \frac{4 \cdot \pi \cdot l \cdot R}{1 + \frac{2l}{\sqrt{l^2 + 4d^2}} - \frac{2l}{\sqrt{(4l)^2 + 4d^2}}}, \quad (1)$$

with the penetration depth d being much smaller than the electrode distance l the following results:

$$\rho_r = 2 \cdot \pi \cdot l \cdot R. \quad (2)$$

2.1.2 | The Wenner method

Using the Wenner method, all electrodes have the same distance from one another. The resistance of the subsurface is measured with two feeding and two measuring electrodes, whereby the measuring electrodes remain fixed, and the position of the feeding electrodes is varied symmetrically around the centre point. The same mathematical relation as per Equation (2) applies. The Wenner method is specified in IEEE Standard 81-1983 Part 1, as well as BS EN 50522.^[25,26]

2.1.3 | The dipole–dipole array method

The voltage and current electrodes each form a dipole at a greater distance from each other.^[27]

2.1.4 | The pole–dipole forward and reverse array method

The voltage electrodes form a dipole. One current electrode is at a greater distance from the voltage electrodes, and the second current electrode is at infinity.^[28]

ERT has been applied to assess fluids with complex, non-Newtonian rheology. Applications include the use of ERT technology to monitor mixing rheology,^[29] with particular interest towards the assessment of slurries (suspension systems).^[30,31] The technology has also been tested on products relevant to fast-moving consumer goods, including yogurts^[32] and shampoos.^[33] While proven as a technology to deliver accurate in-line rheology, there are drawbacks, including limitations to measurements in the presence of laminarity, high energy consumption needs, and restrictions in depth resolution.

2.2 | Ultrasound velocimetry

Ultrasound velocimetry is a non-invasive method used to measure fluid velocity and flow. It is based on the principles of ultrasound technology and is widely used in various applications, including medical diagnosis, industrial process control, and environmental monitoring.

The basic physics behind ultrasound velocimetry is the measurement of the time difference between the emission and reception of ultrasound waves by a transducer.^[14] When ultrasound waves travel through a fluid, the velocity of the fluid affects the speed at which the

waves propagate. By measuring the time delay between the emission and reception of ultrasound waves, the velocity of the fluid can be determined. This is known as the Doppler effect, where the shift in frequency of a wave is proportional to the relative velocity between the source of the wave and the observer.

In ultrasound velocimetry, a transducer is used to emit and receive ultrasound waves, and the time delay between the emission and reception of the waves is measured using electronic circuitry. The velocity of the fluid is then calculated based on the measured time delay and the known speed of sound in the fluid. The velocity of the fluid can be measured at various points along the fluid flow to determine the flow rate and pattern.

Ultrasound velocimetry technology is used along with pressure drop measurements to monitor the fluid rheology of complex fluids,^[34,35] and it has been tested on shampoos.^[36] Low-powered ultrasound technologies are classified as non-destructive. Being an emitter–receiver system, these systems are also often referred to as active AE systems.^[37]

In industrial applications, ultrasonic waves are pulsed in short bursts into the fluid, after which the fluid propagates the ultrasonic wave. A key assumption for ultrasound velocimetry is the presence of heterogeneity. If there are solid particles or bubbles present in the sound field, the sound wave will be scattered or absorbed by these particles or bubbles. Part of the sound energy, which depends on the size and emission characteristics of the particle/bubble, is scattered back to the ultrasonic transducer.

To determine the spatially resolved particle/bubble velocity present in the fluid, the signal reaching the receiver is split into intervals, classified as the sound propagation time according to the respective distance from the transducer. The Doppler frequency shift between the transmitted signal and that of the distance-dependent section of the echo signal is approximately proportional to the particle/bubble speed in the respective measuring depth. This follows the general equation for the Doppler frequency shift, which can be written as follows:

$$f' = \frac{f(c \pm v_D)}{(c \mp v_S)}, \quad (3)$$

with f being the transmission frequency, f' being the receiving frequency, c being the speed of sound, v_D being the speed of the detector in relation to the propagation medium, and v_S being the speed of the detector in relation to the speed of the transmitter in the medium of propagation.^[14,38,39]

However, there are multiple weaknesses in the technology. Standard Doppler velocimetry is only capable of measuring the velocity parallel to the ultrasound beam. Under the assumption of parallel flow, this only works when the angle between the ultrasound beam and the flow direction is known, and there is a direct proportionality between the velocity component and the velocity magnitude. In practical terms, this makes it necessary to pre-condition the flow before passing it by the transducer, or devices cannot be installed at restrictions, openings, or curves. Theoretically, an angle correction can be done; however, it has been reported to remain prone to error.^[40,41]

The other obvious challenge is that there are limits to the degree of gas and/or solid presence possible in the fluid before signal loss occurs, as the wave is either fully scattered or absorbed before propagating to the receiver.

3 | MATERIALS AND METHODS

3.1 | Fluid flow system

A laboratory fluid recirculation system has been used for the data acquisition campaign. All pipework is executed in DN25 316SS (1 in. internal diameter and a pipe segment manufactured from 316 grade stainless steel). The inner piping has been polished to 24–40 Ra, making the pipework hydraulically smooth.

The instrumentation diagram is presented in Figure 1.

A top view of the modified pipe segment with the placed sensor is given in Figure 2.

During the data acquisition campaigns, the sensor has been mounted onto the pipe segment, ensuring a firm positioning. An ultrasound hydrogel (Barclay Swann T/A Econogroup, UK) has been used as a coupling agent between the sensor's sensitive ceramic face and the plateau on the pipe segment.

The fluid is moved by a SPX TA-15BSH-FDA diaphragm pump (Johnson Pump/SPX Flow Inc, USA) that is powered by compressed air (external compressor, Atlas Copco, Sweden). The flow is quantified using an OG4 oval gear flowmeter (TITAN Enterprises Ltd, United Kingdom), being a type of flowmeter which is able to cope with a range of non-Newtonian fluids and which is often deployed in the petrochemical sector.^[42,43] The pressure drops over the length of the modified pipe segment have been read from an analogue dial. During the experiments, the propeller type agitator of the jacketed vessel as set to 500 rpm (IKA-Werke GmbH & CO. KG, Germany).

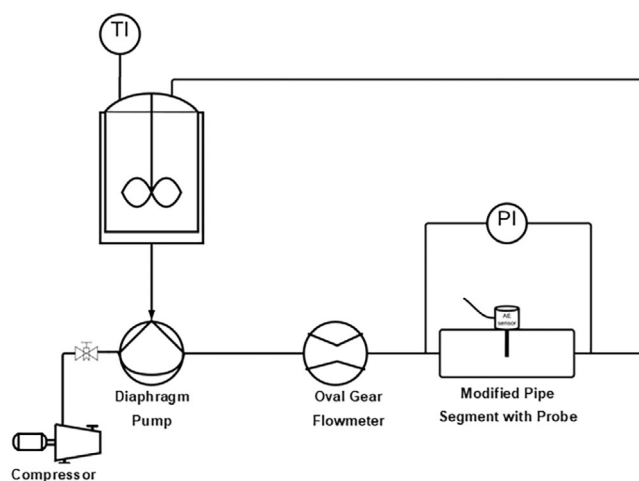


FIGURE 1 Instrumentation chart of the fluid recirculation system with indication of AE sensor location on the outer pipe wall.



FIGURE 2 Top view on the pipe segment with acoustic emission (AE) sensor (sensor flange removed).

3.2 | Fluid preparation

All fluids have been prepared on the same day of usage except for the Carbopol[®] (The Lubrizol Corporation, USA) mixtures as Carbopol[®] requires long dispersion times. Glycerol was sourced from Sigma-Aldrich (Germany) and carboxymethyl cellulose (CMC) was sourced from Thermo Fisher Scientific Inc. (USA).

Based on a wt./wt.% ratio, the following fluids have been mixed in with distilled water:

- 3× Glycerol 70 wt.%, 80 wt.%, and 99 wt.%
- 3× CMC 0.1 wt.%, 0.2 wt.%, and 0.3 wt.%
- 3× Carbopol[®] 0.1 wt.%, 0.15 wt.%, and 0.2 wt.%

The pH of the Carbopol[®] dispersions has been adjusted just before loading the fluid recirculation system and has been set to pH = 4.5 by adding a solution of 1 M NaOH_(l).

3.3 | Fluid rheology determination

A rotational Discovery HR-1 rheometer (TA[®] Instruments, Inc., USA) has been used to characterize the rheological profile for each of the test fluids. The instrument has been recalibrated prior to use (rotational mapping, inertial forces, friction forces, and temperature). This rheometer offers interchangeable geometries, and a 60 mm diameter SS 2° cone-on-plate geometry has been used. The Peltier element for temperature control has been set

to the temperatures as they were present in the fluid recirculation system at the given time of experiment. The fluids were tested for shear rates ranging from 0.1 to 1000 s⁻¹. This information is used as reference to distinguish the different type of fluids and flow conditions.

The rheological parameters of all the fluids are presented in Table 1.

3.4 | Electronics setup of AE

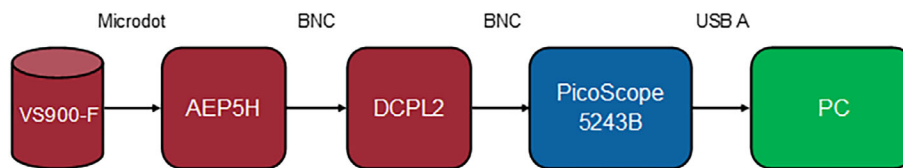
The electronics of the AE detection system (Vallen Systeme GmbH, Germany) comprise a VS900-F passive AE sensor with an IP68 rating ($D \times H$ [mm] = 22.3 × 18.2, sensitive area of ceramic wear plate: $D = 20.3$ mm)

TABLE 1 Summary of the results obtained from the off-line rheometer.

Fluid	Run number	Viscosity (Pa s)	Power law index	Yield stress (Pa)	Rheological model	Temperature (°C)
Glycerol 70 wt.%	Run 1	0.016			Newtonian	27.5
Glycerol 70 wt.%	Run 2	0.017			Newtonian	27.5
Glycerol 70 wt.%	Run 3	0.019			Newtonian	28.5
Glycerol 80 wt.%	Run 1	0.032			Newtonian	20.5
Glycerol 80 wt.%	Run 2	0.032			Newtonian	26.0
Glycerol 80 wt.%	Run 3	0.034			Newtonian	27.0
Glycerol 99 wt.%	Run 1	0.158			Newtonian	20.5
Glycerol 99 wt.%	Run 2	0.158			Newtonian	20.5
Glycerol 99 wt.%	Run 3	0.158			Newtonian	20.5
CMC 0.1 wt.%	Run 1	0.017	0.840		Power law	30.5
CMC 0.1 wt.%	Run 2	0.018	0.835		Power law	31.5
CMC 0.1 wt.%	Run 3	0.011	0.924		Power law	33.5
CMC 0.2 wt.%	Run 1	0.031	0.826		Power law	28.5
CMC 0.2 wt.%	Run 2	0.014	0.988		Power law	30.5
CMC 0.2 wt.%	Run 3	0.027	0.826		Power law	33.0
CMC 0.3 wt.%	Run 1	0.093	0.762		Power law	25.6
CMC 0.3 wt.%	Run 2	0.072	0.788		Power law	29.0
CMC 0.3 wt.%	Run 3	0.052	0.766		Power law	30.0
Carbopol 0.1 wt.%	Run 1	9.70E-03	0.912	7.66E-03	Herschel–Bulkley	26.0
Carbopol 0.1 wt.%	Run 2	9.75E-03	0.845	7.63E-03	Herschel–Bulkley	26.0
Carbopol 0.1 wt.%	Run 3	9.20E-03	0.894	9.05E-03	Herschel–Bulkley	27.0
Carbopol 0.15 wt.%	Run 1	0.192	0.640	0.277	Herschel–Bulkley	24.0
Carbopol 0.15 wt.%	Run 2	0.141	0.662	0.118	Herschel–Bulkley	25.0
Carbopol 0.15 wt.%	Run 3	0.078	0.713	0.026	Herschel–Bulkley	27.0
Carbopol 0.2 wt.%	Run 1	0.903	0.549	3.430	Herschel–Bulkley	22.0
Carbopol 0.2 wt.%	Run 2	0.821	0.542	2.231	Herschel–Bulkley	24.5
Carbopol 0.2 wt.%	Run 3	0.945	0.485	1.254	Herschel–Bulkley	28.0

Abbreviation: CMC, carboxymethyl cellulose.

FIGURE 3 Acoustic emission (AE) system setup schematic. BNC, Bayonet Neill–Concelman; USB A, universal serial bus.



(Figure 3). This sensor has a broadband frequency response, peaking at 150 and 350 kHz.

As this sensor does not possess a built-in amplification unit, the sensor has been connected via a microdot connector to an AEP5H preamplifier (Vallen Systeme GmbH, Germany) with a gain of 34 dB. The AEP5H preamplifier (Vallen Systeme GmbH, Germany) is connected via a 300 mm long BNC-terminated cable to a DCPL2 decoupling unit, which delivers the voltage required for the sensing system and decouples the sensor signals internally.

To record the AEs, a PicoScope 5243B oscilloscope (Pico Technology Ltd, UK) has been connected to the AE detection system (BNC-type cable), which is further connected to a personal computer (USB type A connection).

3.5 | Signal acquisition

The acquisition parameters have been set using PicoScope6 software (version 6.14.23.5207, Pico Technology Ltd, UK). One hundred recordings per flow rate per fluid were taken once the fluid reached steady-state flow. Steady state was defined as the point at which no flow rate variation had been observed for 30 consecutive seconds.

All signals were acquired with PicoScope6 software, and the raw data was captured in the time domain. Each recording resulted in a buffer length of 500 ms (also known as recording or page length), with the sample interval set to 848 ns. This equated to a sampling frequency of 1.179 MHz or 589,623 individual data points per 500 ms of recording. All experiments were repeated three times. A temperature oscillation of 0.5°C was observed, despite the system being jacketed.

Data were acquired for the following steady-state flow scenarios. The Reynolds numbers for the power law fluid and Herschel–Bulkley fluid were calculated using the equations presented in^[44] (Table 2):

3.6 | Post-acquisition data processing

3.6.1 | Fourier transform

All acquired data points of the fluid flow experiments have been processed using MATLAB R2020b Update 6 64-bit edition software (MathWorks Inc, USA).

Time domain data (voltage fluctuations over time) has been modelled into the frequency domain by applying a discrete Fourier transform.

Mathematically, for a vector X and Y of length n , this is achieved as by Bosch,^[45] Frigo and Johnson,^[46] Johnson and Frigo^[47]:

$$X(j) = \frac{1}{n} \sum_{k=1}^n Y(k) \times e^{-2\pi i/n - (j-1)(k-1)}, \quad (4)$$

$$Y(k) = \frac{1}{n} \sum_{j=1}^n X(j) \times e^{-\frac{2\pi i}{n} - (j-1)(k-1)}, \quad (5)$$

where $e^{-2\pi i/n}$ is one of the n *de Moivre* numbers. The *de Moivre* number is a complex number represented as $\cos(\theta) + i\sin(\theta)$, where θ is an angle in radians and i is the imaginary unit (square root of -1).

3.6.2 | FFT feature-based flowrate regression

Fourier-transformed signals were simplified to draw conclusions about the relationship between flow rate and the frequency domain. Since the frequency domain of the signals contained approximately 524,000 individual frequencies over 900 recordings per fluid, it was necessary to condense the data to a manageable amount for further computation. An arithmetic mean was created for every 1000 columns, resulting in a 900×534 matrix. The rationale behind this processing step was to combine the information-rich signal into chunks of averaged data, leading to a coarse resolution Fourier transform spectrum while retaining enough information for further regression.

Regressions were performed using a nonlinear autoregressive network with exogenous inputs (NARX) neural network (MathWorks Inc, USA). The model was created using a scaled conjugate gradient to reduce the computational power required. The NARX neural network architecture is widely used for modelling dynamic systems with time-varying inputs and outputs. NARX models are composed of two structures: a nonlinear autoregressive (AR) structure and an exogenous input (X) structure. The AR structure models the dependencies between the outputs and past inputs and outputs of a system, while the X structure models the dependencies between the outputs and external inputs that do not originate from the system itself.

TABLE 2 Fluid state summary at point of data acquisition.

Run number	Fluid	Relative temperature (°C)	Repeat	Steady state flowrate (lpm)	Pressure drop (bar)	Reynolds number
1	Glycerol 70 wt.%	28.0	M	32.2	0.15	2030
		27.5	1	32.1		
		27.5	2	31.9		
2	Glycerol 70 wt.%	27.5	M	41.7	0.20	2503
		27.5	1	41.7		
		28.0	2	42.6		
3	Glycerol 70 wt.%	28.0	M	48.1	0.25	2575
		28.5	1	48.4		
		28.5	2	48.4		
1	Glycerol 80 wt.%	20.5	M	29.9	0.18	966
		20.5	1	29.6		
		20.5	2	29.6		
2	Glycerol 80 wt.%	26.0	M	39.8	0.25	1297
		26.0	1	39.8		
		26.0	2	40.0		
3	Glycerol 80 wt.%	27.0	M	46.4	0.30	1407
		27.0	1	45.9		
		27.0	2	45.7		
1	Glycerol 99 wt.%	20.5	M	16.8	0.30	115
		20.5	1	16.7		
		20.5	2	16.8		
2	Glycerol 99 wt.%	20.5	M	26.6	0.45	183
		20.5	1	26.7		
		20.5	2	26.9		
3	Glycerol 99 wt.%	20.5	M	33.3	0.58	231
		20.5	1	33.7		
		20.5	2	34.0		
1	CMC 0.1 wt.%	30.5	M	33.3	0.09	1.37E+06
		30.5	1	3.3		
		31.0	2	33.7		
2	CMC 0.1 wt.%	31.0	M	44.1	0.13	1.79E+06
		31.5	1	44.5		
		32.0	2	44.5		
3	CMC 0.1 wt.%	32.5	M	48.8	0.15	2.00E+06
		33.0	1	48.8		
		33.5	2	48.8		
1	CMC 0.2 wt.%	29.0	M	33.9	0.10	7.43E+05
		29.0	1	34.1		
		29.5	2	33.9		
2	CMC 0.2 wt.%	30.0	M	43.7	0.15	2.62E+06
		30.5	1	43.9		
		31.0	2	43.8		

TABLE 2 (Continued)

Run number	Fluid	Relative temperature (°C)	Repeat	Steady state flowrate (lpm)	Pressure drop (bar)	Reynolds number
3	CMC 0.2 wt.%	31.5	M	48.4	0.15	1.30E+06
		32.0	1	48.7		
		33.0	2	48.7		
1	CMC 0.3 wt.%	25.0	M	33.0	0.14	2.23E+05
		25.6	1	33.3		
		26.2	2	33.4		
2	CMC 0.3 wt.%	27.0	M	43.3	0.17	4.11E+05
		28.0	1	3.5		
		29.0	2	43.3		
3	CMC 0.3 wt.%	29.0	M	48.4	0.2	6.36E+05
		29.5	1	48.4		
		30.0	2	48.2		
1	Carbopol 0.1 wt.%	26.0	M	34.3	0.09	4.87E+03
		26.0	1	34.3		
		26.0	2	34.3		
2	Carbopol 0.1 wt.%	26.0	M	44.5	0.13	9.52E+03
		26.0	1	44.5		
		26.0	2	44.3		
3	Carbopol 0.1 wt.%	26.5	M	49.7	0.15	8.55E+03
		26.5	1	49.6		
		27.0	2	49.6		
1	Carbopol 0.15 wt.%	24.0	M	32.8	0.11	1.03E+03
		24.5	1	32.8		
		25.0	2	32.8		
2	Carbopol 0.15 wt.%	25.0	M	44.5	0.15	1.91E+03
		25.0	1	44.5		
		25.5	2	44.5		
3	Carbopol 0.15 wt.%	26.0	M	50.0	0.18	3.01E+03
		26.5	1	50.0		
		27.0	2	50.0		
1	Carbopol 0.2 wt.%	22.0	M	30.8	0.19	3.08E+02
		23.0	1	31.0		
		23.5	2	31.1		
2	Carbopol 0.2 wt.%	24.0	M	42.2	0.22	5.75E+02
		24.5	1	42.7		
		25.0	2	42.9		
3	Carbopol 0.2 wt.%	26.0	M	49.9	0.25	9.23E+02
		27.0	1	49.9		
		28.0	2	49.8		

Abbreviations: CMC, carboxymethyl cellulose; M, measurement.

NARX models have a wide range of applications, including process control, system identification, and time series prediction. In process control, NARX models can be used to model the relationships between control inputs and process outputs, enabling effective control of the system. In system identification, NARX models can be used to estimate the parameters of a system's dynamic model based on input-output data. In time series prediction, NARX models can be used to predict future values of a system's outputs based on past inputs and outputs.

NARX models are trained using supervised learning, where a set of input-output data is used to learn the model parameters. The performance of NARX models is evaluated by testing the models on new, unseen data. The optimization of NARX model parameters can be performed using various optimization algorithms, including gradient descent and genetic algorithms.

Regressions were created using 70% randomly selected data, while the remaining 30% were used equally to validate and test the regression models. The choice of NARX is justified as this type of network is specifically designed to create nonlinear regression models for time series data obtained through the measurements of the AE sensor and is commonly used for empirically collected information.^[48,49]

3.6.3 | Rheology-AE comparison

To probe the relationship between AE response to rheology, the Fourier spectrum has been divided and

averaged into three equal parts. This allows to set AE into relationship against the fluid rheology by applying the relevant fluid model to all fluids (i.e., Newtonian model for glycerol). In a final step, the quotient between the vectors containing the simplified AE information, each of the chunks of total accumulated peak intensity, and the relative fluid model fluid variables (values as per Table 2) has been created and plotted (MathWorks Inc, USA) (Figure 4).

4 | RESULTS AND DISCUSSION

4.1 | Signal reproducibility

Once steady state was reached, data was collected in triplicate. Steady state was defined as the point at which flow rates did not fluctuate for 30 consecutive seconds. The figure below presents the AEs in their frequency domain for all three fluids (Figure 5).

Figure 5 shows the average frequency spectra of 100 buffers per signal capture campaign. All three figures exhibit close matches between measurement and repeats 2 and 3. However, more variation appears within the power law fluid case. An obvious deviation in Figure 5B appears for measurement, while repeats 1 and 2 exhibit close matches and overlay (see the frequency range between 10^3 and 10^4 Hz). A potential reason for the shift in frequency may be the temporary fluctuation of pressure drop within the fluid recirculation system, leading to changes in transient energy releases. This assumption is

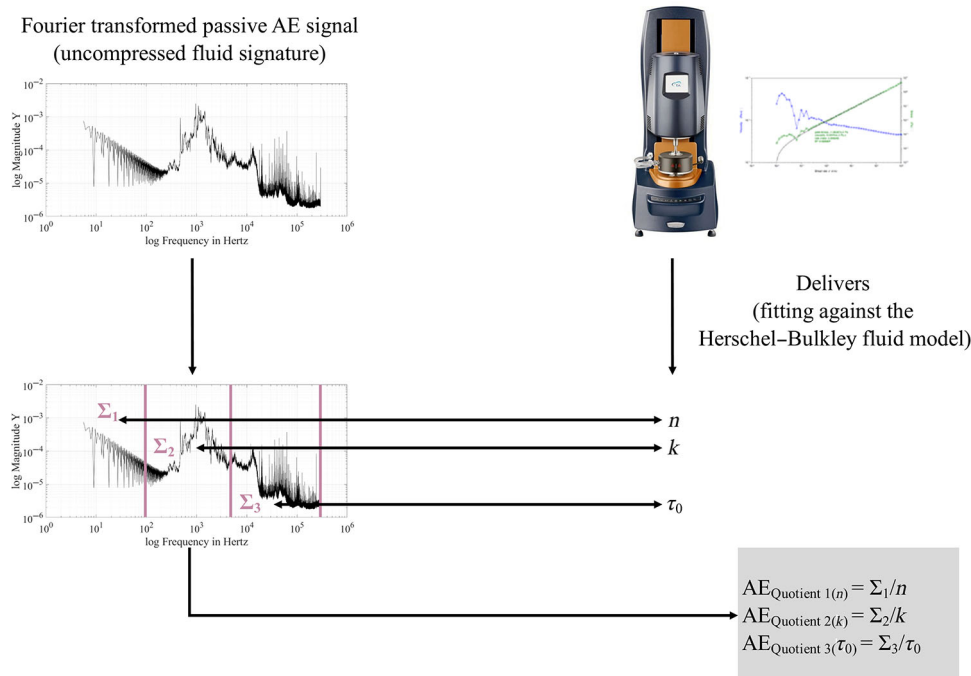
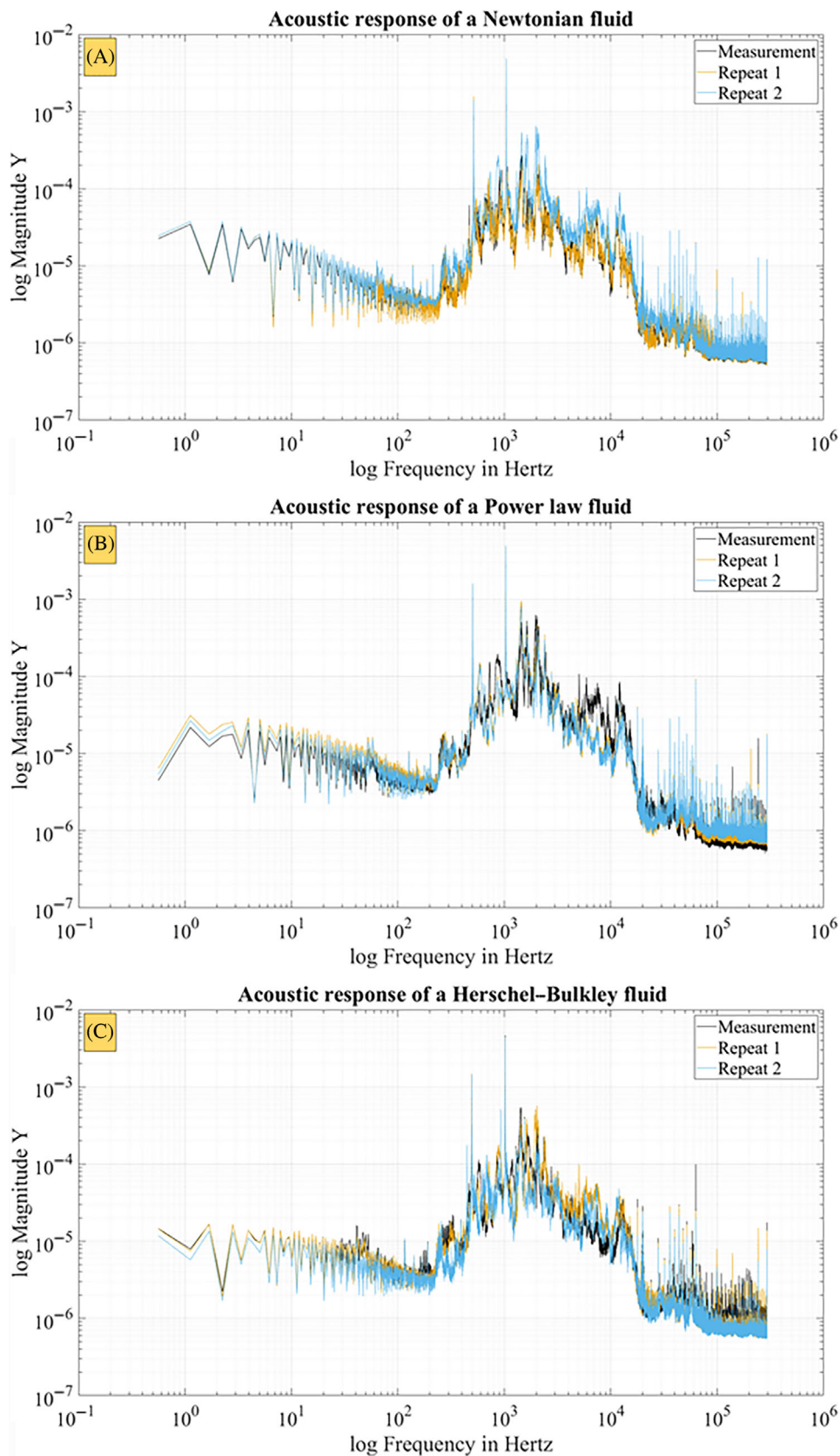


FIGURE 4 Principal schematic for the determination of the rheology-AE quotient.

FIGURE 5 Frequency domains of averaged frequency domain signals ($n = 100$ per run) for all three fluid types on a given flowrate. Labelling applies as per Table 2.



in agreement with the literature, which reports that AEs are influenced by pressure fluctuations.^[50] However, this must be considered with caution given that the

magnitude order of 10^7 introduces measurement uncertainties, as this magnitude order approaches the lowest resolution limits of the AE sensor.

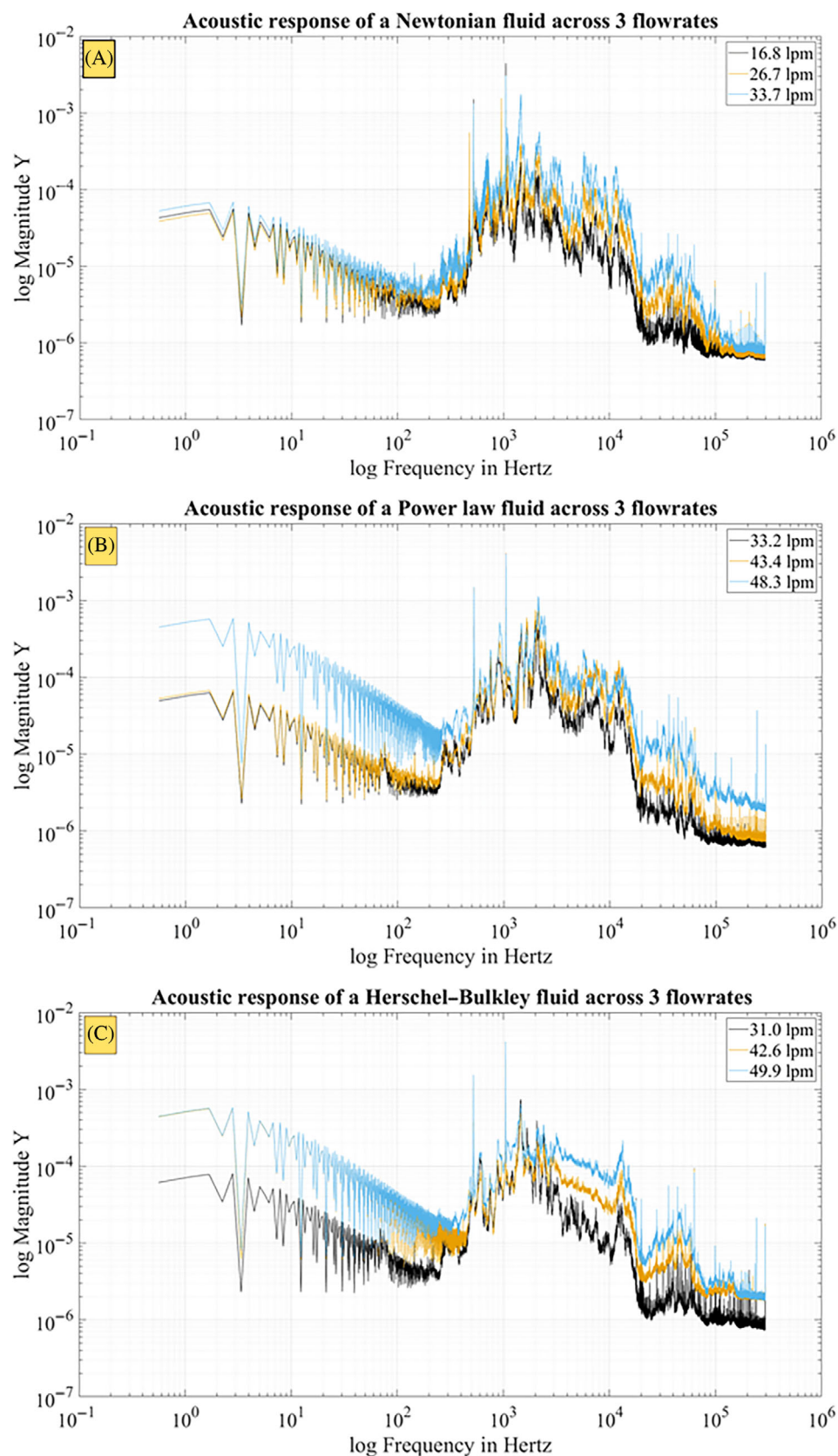


FIGURE 6 Frequency domains of averaged frequency domain signals ($n = 300$ per flowrate) for all three fluid types on a varying flowrate. (A) represents glycerol, (B) represents carboxymethyl cellulose (CMC), and (C) represents carbopol[®].

For Figure 5A, a deviation between measurement and repeat 1 versus repeat 2 is apparent. Given that the chosen Newtonian fluid is a dilution of glycerol, it is very

likely that the inner friction during pumping may have increased the fluid temperature and caused this slight shift in the AE pattern. Further, glycerol is highly

hygroscopic, hence the fluid properties may have changed over time. This is a plausible cause, given that the study location does not have the means to control environmental conditions.

In general, passive measurements of AEs are bulk readings composed of multiple factors, including the energy released through thermal load change.^[51] This makes it very difficult to deliver definite answers on the reasons for variation. However, the impacts of temperature and pressure fluctuations are drawn from literature studying AEs released from solid matter since passive AE measurements have not been previously studied on pure fluid flow applications of complex fluids. Again, another variable of uncertainty must be taken into consideration when interpreting the results.

The Herschel–Bulkley fluid (Figure 5C) exhibits the best overlay of averaged frequency domains, meaning that this fluid has probably maintained steady state best when compared to the power law and Newtonian cases.

4.2 | Flowrate effects

The following section presents the changes in AE in response to increases of the flowrate (Figure 6). Flowrates are indirectly defined by pump air pressure supplied. Each increase step in flowrate equates to 2, 4, and 6 bar of air pressure applied to the pump.

Regardless of rheology, increases in flowrate lead to increases in peak intensity (Figure 6). A similar observation has been made for obstructed pipe flow with

water as a working fluid in a recirculation loop (Newtonian fluid).^[5] Studies on leak detection, along with the analysis of frequency domains, also show that a drop in pressure, hence a drop in flowrate, leads to reduced energy levels expressed by the peak intensity.^[52] For all three fluids (3×300 buffer, as per Table 2) across all formulations, flowrate rise (2, 4, and 6 bar pump working pressure) versus maximum peak intensity can be put into stepwise regression (Table 3). This means that the reduced Fourier transform spectra contain enough information to allow drawing conclusions on flowrate. This would also mean that a single passive AE sensor could be trained to measure fluid flow rheology-independently, hence being advantageous to traditional electromagnetic and Coriolis flowmeters that cannot deliver accurate readings on flowrate of complex rheology fluids.

4.3 | Rheology effects

Varying rheology expresses itself macroscopically in changes of flow resistance and behaviour. When analyzing the frequency of different model fluids of modified rheology, changes are apparent as well (Figure 7).

Despite being unique in acoustic fingerprints, there is no obvious correlating relationship apparent between formulation changes (rheology manipulation) and the resulting frequency domain. However, relationships can become apparent when creating the quotient of rheological factor to the frequency domain (Figure 8).

It can be seen that with an increase of rheology complexity (Newtonian, power law, Herschel–Bulkley), the data becomes more scattered. In particular, scattered effects become apparent when examining the quotient n from the Herschel–Bulkley model. However, across all 9 formulations, increases in viscosity are well reflected within the data. Further, the data are reliable when analyzing the quotient for the yield stress. Overall, the assumption of a relationship between AE and rheology is reasonable given the unique acoustic fingerprints and results of Figure 7. There is, however, a need to tune the third rheological factor regarding AE or to identify other modes of feature extraction. Alternatively, a sensor that is better suited to the resolution window of observation may be able to deliver data that is less prone to fluctuation. Yet, it must be kept in mind that this quotient is formed by dividing live sensor information with a static value retrieved from an off-line rheometer. Therefore, the data variation may be genuine given that the off-line measurement does not deliver a picture of the fluid's current state as it

TABLE 3 Neural network regression outputs for all nine fluids ($n = 300$ per fluid per flowrate).

Fluid	NARX regression function	R^2 value
Glycerol 80 wt.%	Output $\cong 0.98 \cdot \text{Target} + 1.10$	0.99
Glycerol 90 wt.%	Output $\cong 1.00 \cdot \text{Target} + 0.15$	1.00
Glycerol 99 wt.%	Output $\cong 0.98 \cdot \text{Target} + 0.45$	0.96
CMC 0.1 wt.%	Output $\cong 0.98 \cdot \text{Target} + 0.39$	0.99
CMC 0.2 wt.%	Output $\cong 0.99 \cdot \text{Target} + 0.35$	0.99
CMC 0.3 wt.%	Output $\cong 0.98 \cdot \text{Target} + 0.70$	0.99
Carbopol 0.10 wt.%	Output $\cong 0.97 \cdot \text{Target} + 1.00$	0.99
Carbopol 0.15 wt.%	Output $\cong 0.96 \cdot \text{Target} + 1.70$	0.97
Carbopol 0.20 wt.%	Output $\cong 0.99 \cdot \text{Target} + 0.21$	1.00

Note: Input, given flowrate and outputs, maximum peak intensity (maximum voltage gain within the acoustic spectrum).

Abbreviation: CMC, carboxymethyl cellulose; NARX, nonlinear autoregressive network with exogenous inputs.

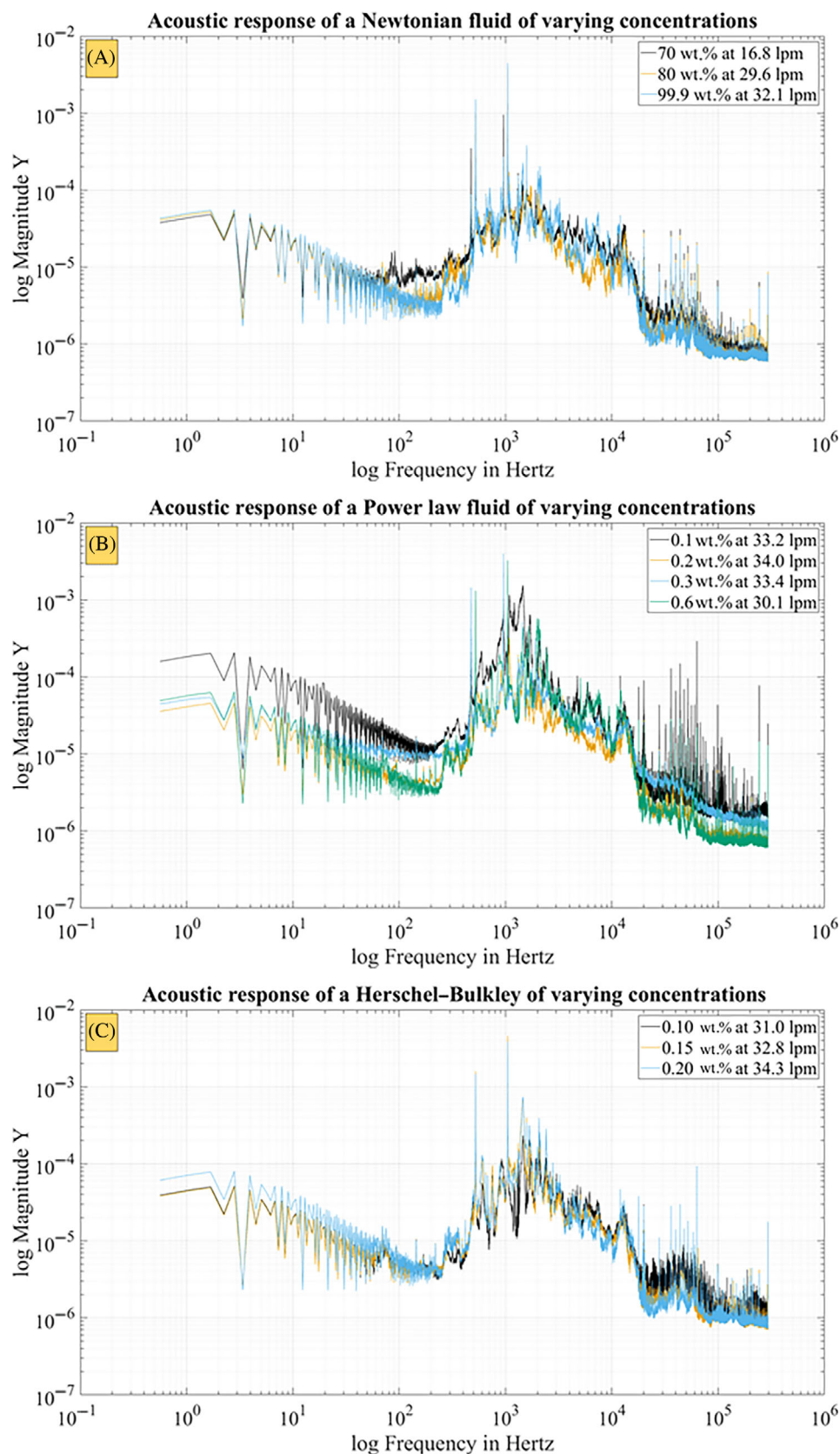
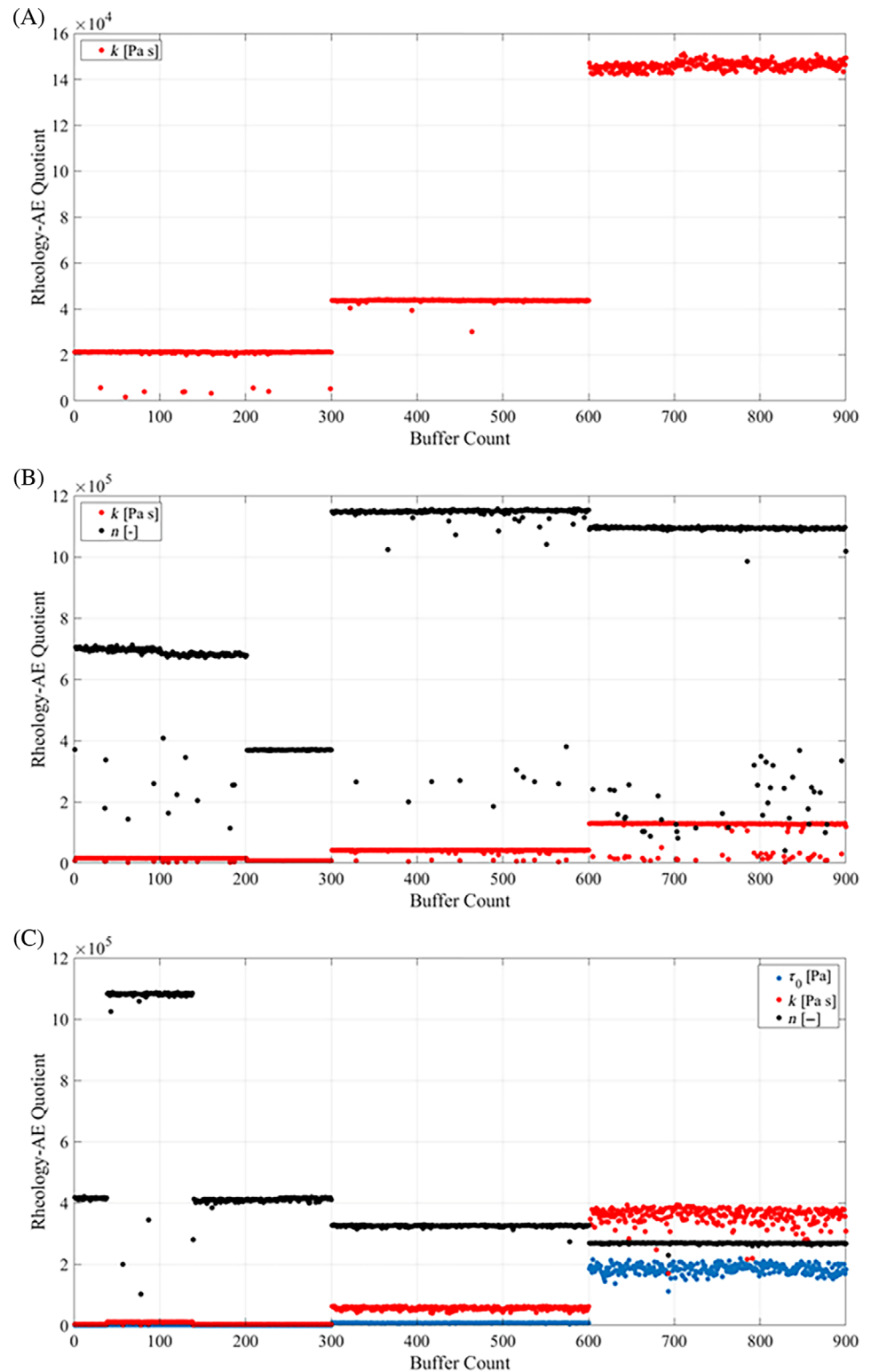


FIGURE 7 Frequency domains of fluid groups of altered rheology (A, Newtonian; B, power law; and C, Herschel–Bulkley). Each incremental flowrate increase corresponds to a pump working pressure of 2, 4, and 6 bar, respectively.

passes the duct. There may have been fluctuations in the compressor performance for the displayed 50 s (affecting the pump's flowrate directly). Therefore, given

the high sensitivity of the sensor, there could have been a temporary change of the rheological state of the fluid during this period.

FIGURE 8 Rheology-AE correlation plots for (A) Newtonian (Buffer number: 1–300: Glycerol 70 wt.%, 301–600: Glycerol 80 wt.%, 601–900: Glycerol 99 wt.%); (B) power law (Buffer number: 1–300: CMC 0.1 wt.%, 301–600: CMC 0.3 wt.%, 601–900: CMC 0.3 wt.%), and (C) Herschel–Bulkley (Buffer number: 1–300: Carbopol[®] 0.1 wt.%, 301–600: Carbopol[®] 0.15 wt.%, 601–900: Carbopol[®] 0.2 wt.%).



5 | CONCLUSION

A single passive AE sensor has been installed on the outer wall of a modified, straight pipe segment. The presented, patented system has been specifically designed to detect AE releases from a fluid as it passes through such

a modified duct. The entire system has been successfully subjected to patenting.

The results indicate that the system can generate unique acoustic fingerprints for fluids of different rheology. Further, the system indicates that increases in flow-rate lead to an increase in the number of AEs.

This work has proven the system's functionality on a granular scale; however, it would be desirable for future work to compare time resolved temperature and pressure fluctuation readings versus the AEs collected. Currently, this is not feasible with the existing rig setup, and would require modifications to the fluid recirculation system. The biggest limitation is the reliance on comparing off-line gathered information against live and in situ information collected by a highly sensitive AE sensor. The sensor captures live data of a fluid's state every 500 ms while a rotational rheometer is (i) not able to replicate this state in a true manner and (ii) would not have the capacity to deal with sudden changes in the system, such as temporary pressure drops lasting only a very short duration.

While the rheology–AE quotient has shown high sensitivity, this model could be improved by using more complex rheological models such as the Cross model. This would be beneficial when a process is covering a range of shear ranges with fluids which may exhibit more complex rheological behaviour, or the Casson model given the high Reynolds numbers present in the fluid recirculation system. This limitation is due to the available computational power, given that the more constituents an equation possesses, the more data splits must be exercised. In practical terms, this means that additional memory is required, which may raise questions about whether this is feasible if implemented in processing lines across various positions. However, considering the overall aim to utilize fluids of different rheological profiles, power law and Herschel–Bulkley are still sufficient for this purpose. Mapping these various fluids against changes in AE seems to be possible; however, the approach presented in this paper is a starting point that will allow for further investigation into other frequency spectrum divisions. Nevertheless, the general trend of AE changes in response to fluid rheology remains evident.

In conducting such a study, it would unlock the possibility of understanding how pressure fluctuations under constant temperature, or vice versa, could drive changes in the frequency domain, allowing for the creation of predictive models on the composition of fluid-released AEs. However, enhancing time resolution leads to significant increases in data points, and it would become necessary to move larger computation clusters to process the data. This might be interesting from a knowledge generation point of view; however, it might not be desirable for the development of a technology that could serve in industrial settings since companies are unlikely to have exceptional computational power on site.

This could also help with the development of modelling software since there is currently no CFD software package available to simulate passive AEs, which

remains a gap in the literature. Current software packages are well-equipped to cope with active AE measurements (ultrasound-based) as they rely on a reference frequency in their input. The chances of this happening in the foreseeable future are slim, given the fairly low interest in passive AE measurements compared to ongoing work in the field of ultrasound technologies. This is mainly due to the reality that ultrasound-based techniques are much more studied, and having a transduced reference signal makes it very easy to derive conclusions on the interaction between energy input and fluid interaction, while passive AE measurements are bulk readings. Furthermore, this is a technology that has a long-standing tradition in solid matter construction and civil engineering, and moving into the field of fluid flow is breaking new ground.

The only passive AE systems of common industrial application are, in general, array-based, meaning they are more costly when compared to ultrasound technologies. However, passive AE offers a clear advantage as there are no risks of signal loss between transducer and receiver, which is a key limitation of ultrasound-based technologies. Such systems can only cope to a certain degree with the presence of bubbles, solids, and long distances. Having a modified pipe segment with an extending probe makes the presented solution fully scalable as desired.

Furthermore, the presence of bubbles and solids enhances signal strength for passive systems. This makes it a likely candidate technology for becoming more prevalent in the assessment of dispersion and multiphase systems.

AUTHOR CONTRIBUTIONS

Daniel Ingo Hefft: Conceptualization, data curation, formal analysis, investigation, methodology, writing – original draft, writing – review and editing. **Federico Alberini:** Funding acquisition, project administration, supervision, validation, writing – review and editing.

ACKNOWLEDGEMENTS

The authors wish to acknowledge Dr. Cyrus John Espinoza for assisting in the data collection during his induction period.

CONFLICT OF INTEREST STATEMENT

The authors have no conflicts to declare.

DATA AVAILABILITY STATEMENT

The authors select not to share data to protect filed IP.

ETHICS STATEMENT

No human subjects were part of this study. No animal subjects were part of this study. This study complies with

the regulations and ethical guidelines of the University of Birmingham.

ORCID

Daniel Ingo Hefft  <https://orcid.org/0000-0002-0775-7538>

REFERENCES

- [1] J. Aho, S. Hvidt, S. Baldursdottir, *Analytical Techniques in the Pharmaceutical Sciences*, Springer, New York **2016**, p. 719.
- [2] A. Mohamed, S. Salehi, R. Ahmed, *Geothermics* **2021**, 6(93), 102066.
- [3] G. Tabilo-Munizaga, G. V. Barbosa-Cánovas, *J. Food Eng.* **2005**, 67(1-2), 147.
- [4] Y. J. Zheng, X. J. Loh, *Polym. Adv. Technol.* **2016**, 12(12), 1664.
- [5] D. I. Hefft, F. Alberini, *Biosyst. Eng.* **2020**, 3(191), 48.
- [6] N. M. C. Martins, A. K. Soares, H. M. Ramos, D. I. C. Covas, *Comput. Fluids* **2016**, 3(126), 129.
- [7] S. P. Sullivan, L. F. Gladden, M. L. Johns, *J. Non-Newtonian Fluid Mech.* **2006**, 133(2-3), 91.
- [8] C. Damian, *Ovidius Univ. Ann. Chem.* **2013**, 24(1), 17.
- [9] W. S. Guan, H. X. Huang, *Polym. Eng. Sci.* **2013**, 53(7), 1563.
- [10] J. M. Rees, *Adv. Colloid Interface Sci.* **2014**, 4(206), 294.
- [11] Fortune Business Insights, *Shampoo Market Size, Share & Covid 19 Impact Analysis*, Fortune Business Insights, Hyderabad, India **2020**.
- [12] F. Alberini, D. I. Hefft, G. G. Forte (WIPO), *UK WO2020260889A1*, 2020.
- [13] L. Baronti, M. Castellani, D. Hefft, F. Alberini, *Can. J. Chem. Eng.* **2022**, 100(3), 521.
- [14] M. J. W. Povey, *Ultrasonic Techniques for Fluids Characterization*, Elsevier, Dubai **1997**.
- [15] D. I. Hefft, F. Alberini, in *2019 AIChE Annual Meeting*, AIChE, Orlando, FL **2019**, p. 2.
- [16] Z. A. Arega, A. Bhasin, W. Li, D. E. Newcomb, E. Arambula, *J. Mater. Civ. Eng.* **2014**, 26(11), 4014078.
- [17] L. P. F. Abreu, J. R. M. Oliveira, H. M. R. D. Silva, D. Palha, P. V. Fonseca, *Constr. Build. Mater.* **2017**, 7(142), 342.
- [18] Henkel AG & Co KGaA, *World Economic Forum Recognizes Henkel as Frontrunner in the 4th Industrial Revolution for the Second Time*, Henkel AG & Co KGaA, Montornès, Spain **2021**.
- [19] A. Lim, 'Massive improvements': Unilever Dubai implements Industry 4.0 system for factory, <https://www.cosmeticsdesign-asia.com/Article/2018/11/28/Massive-improvements-Unilever-Dubai-implements-Industry-4.0-system-for-factory> (accessed: November 2018).
- [20] S. Hammer, *Geophysics.* **1939**, 4(3), 184.
- [21] R. Maillat, *Geophysics.* **1947**, 12(4), 529.
- [22] P. Sava, A. Revil, M. Karaoulis, *Geophys. J. Int.* **2014**, 198(2), 880.
- [23] D. J. Marshall, T. R. Madden, *Geophysics.* **1959**, 24(4), 790.
- [24] F. Wenner, *Bull. Bur. Stand.* **1916**, 12(4), 469.
- [25] British Standards Institute, *BS EN 50522:2010 Earthing of Power Installations Exceeding 1 kV a.c.*, British Standards Institute (BSI), London, UK **2012**.
- [26] IEEE. *IEEE Guide for Measuring Earth Resistivity, Ground Impedance, and Earth Surface Potentials of a Ground System Part 1: Normal Measurements*, IEEE, New York **1983**, p. 1, <https://doi.org/10.1109/IEEESTD.1983.82378>
- [27] T. Pánek, W. Margielewski, P. Tábořík, J. Urban, J. Hradecký, C. Szura, *Geomorphology* **2010**, 123(1-2), 165.
- [28] R. Saad, M. N. Muztaza, M. T. Zakaria, M. M. Saidin, *Journal of Geology & Geophysics* **2017**, 06(1), 1.
- [29] D. Patel, F. Ein-Mozaffari, M. Mehrvar, *AIChE J.* **2014**, 60(1), 315.
- [30] H. Movafagh, G. Turcotte, F. Ein-Mozaffari, *Biofuels* **2016**, 7(4), 365.
- [31] W. Yenjaichon, J. R. Grace, C. J. Lim, C. P. J. Bennington, *Chem. Eng. Sci.* **2012**, 6(75), 167.
- [32] M. Henningsson, K. Östergren, P. Dejmek, *J. Food Eng.* **2006**, 76(2), 163.
- [33] Z. Ren, A. Kowalski, T. L. Rodgers, *Flow Meas. Instrum.* **2017**, 12(58), 31.
- [34] D. Patel, F. Ein-Mozaffari, M. Mehrvar, *IOP Conf. Ser.: Mater. Sci. Eng.* **2012**, 42, 12048.
- [35] S. Saeed, F. Ein-Mozaffari, S. R. Upreti, *Ind. Eng. Chem. Res.* **2007**, 46(7), 2172.
- [36] J. Wiklund, M. Johansson, J. Shaik, P. Fischer, E. Windhab, M. Stading, A.-M. Hermansson, in *Third International Symp. on Ultrasonic Doppler Methods for Fluid Engineering*, EFPL, Lausanne, Switzerland **2002**.
- [37] J. W. R. Boyd, J. Varley, *Chem. Eng. Sci.* **2001**, 56(5), 1749.
- [38] C. Poelma, *Exp. Fluids* **2017**, 58(1), 3.
- [39] E. G. Richardson, in *Ultrasonic Physics* (Ed: A. E. Brown), Elsevier, New York **2013**.
- [40] K. H. Fraser, C. Poelma, B. Zhou, E. Bazigou, M. X. Tang, P. D. Weinberg, *J. R. Soc., Interface* **2017**, 14(127), 20160761.
- [41] K. Logason, T. Bärlin, M. L. Jonsson, A. Boström, H. G. Hårdemark, S. Karacagil, *J. Geophys. Res.: Biogeosci.* **2001**, 21(4), 311.
- [42] M. Meribout, F. Shehzad, N. Kharoua, L. Khezzar, *Measurement* **2020**, 9(161), 107806.
- [43] R. Li, P. Liang, S. Mussmann, in *Proc. of the Fourteenth Annual ACM-SIAM Symp. on Discrete Algorithms*, Society for Industrial and Applied Mathematics, Philadelphia, PA **2020**, pp. 102–121.
- [44] K. Madlener, B. Frey, H. K. Ciezki, *Progress in Propulsion Physics*, EDP Sciences, Les Ulis, France **2009**, p. 237.
- [45] S. Bosch, *Algebra*, 7th ed., Springer Berlin Heidelberg, Berlin **2009**.
- [46] M. Frigo, S. G. Johnson, in *Proc. of the 1998 IEEE International Conf. on Acoustics, Speech and Signal Processing*, ICASSP '98 (Cat. No.98CH36181) vol. 3, IEEE, New York **1998**, pp. 1381–1384.
- [47] S. G. Johnson, M. Frigo, *IEEE Transactions on Signal Processing* **2007**, 55(1), 111.
- [48] J. M. P. Menezes, G. A. Barreto, *Neurocomputing* **2008**, 71(16-18), 3335.
- [49] P. Menezes Jr., G. Barreto, in *2006 Ninth Brazilian Symp. on Neural Networks (SBRN'06)*, IEEE, New York **2006**, p. 28.
- [50] L. Ning, Z. Shicheng, Z. Yushi, M. Xinfang, W. Shan, Z. Yinuo, *Rock Mech.* **2018**, 51(4), 1047.
- [51] Y. Liu, A. Ma, P. Han, Z. Chen, Y. Jia, *Appl. Microbiol. Biotechnol.* **2020**, 104(24), 10531.
- [52] G. Y. Ye, K. J. Xu, W. K. Wu, *Sens. Actuators, A* **2018**, 11(283), 340.

How to cite this article: D. I. Hefft, F. Alberini, *Can. J. Chem. Eng.* **2023**, 1. <https://doi.org/10.1002/cjce.24944>